Investigation of Binary and Ternary Cu−V−Ce Oxides by X-ray Diffraction, Thermal Analysis, and Electron Paramagnetic Resonance

R. Cousin, S. Capelle, E. Abi-Aad,* D. Courcot, and A. Aboukaïs

Laboratoire de Catalyse et Environnement, EA 2598, Université du Littoral−Côte d'Opale, MREID, 145 Avenue Maurice Schumann, F-59140 Dunkerque, France

Received January 18, 2000. Revised Manuscript Received June 15, 2001

The influence of vanadyl and copper precursors, impregnated on ceria, was evaluated by X-ray diffraction (XRD), thermal analysis (TG-DSC), and electron paramagnetic resonance (EPR) of binary and ternary oxides. The formation of a copper oxalate phase from copper nitrate and vanadyl oxalate was revealed during the preparation of the ternary oxide (1Cu1V10Ce). Three types of Cu(II) species in the dried copper containing solids were evidenced: (i) Cu(II) cations with an elongated octahedral symmetry attributed to the copper nitrate precursor, (ii) a copper oxalate phase with a compressed octahedral symmetry and (iii) well-dispersed Cu^{2+} ions on the ceria surface, located in a tetragonally distorted octahedral crystal field and surrounded by less than six ligands. The dispersion of the copper-(II) cations over the ceria support surface was facilitated by the copper nitrate precursor. The EPR intensities clearly show that the increase of the oxalate precursor content induces a large fraction of copper that escapes detection by EPR and could be consistent with the presence of large Cu(II) agglomerates. After the calcination of the solids at 300 °C, only one copper species was evidenced and assigned to Cu^{2+} ions located in octahedral sites tetragonally distorted. The distortion was more pronounced in the presence of vanadium than in the case of the copper cerium oxide samples. The high dispersion of the copper(II) cations over the ceria support surface, owing to the copper nitrate precursor, was confirmed even after its thermal decomposition.

Introduction

Catalytic performances of the metal oxide catalysts are highly dependent on several parameters, such as the type of support, the active phase dispersion, the structural properties, the thermal treatments, the activation conditions, and it is undeniable that the preparation method and the precursors have a major effect on the previous parameters and on the performances of the catalytic materials.[1−5] It has been recently demonstrated[5] that during the preparation of alumina as a catalyst support from aluminum nitrates, $NO_2^{\bullet}$ radicals have been formed in the catalyst after calcination of the solid under air at different temperatures. These radicals remained stable until a calcination temperature of 800 °C. When the calcined catalyst was degassed under vacuum above 300 °C, the $NO_2^{\bullet}$ was reduced to give $NO^{\bullet}$ and O^- species, which were both tightly trapped in the solid.[5] The formation of such unexpected radicals could affect the catalytic properties of solids in the case where they were not previously evidenced.

Cerium(III) hydroxide is commonly prepared by precipitation from cerium(III) nitrate and sodium hydroxide. In presence of oxygen in air, at room temperature, $Ce(OH)_3$ leads to the formation of $Ce(OH)_4$. After calcination of this hydroxide at high temperatures (>400 °C), ceria (CeO_2) is mainly formed, and EPR reveals some Ce^{3+} ions,[6] which are paramagnetic species characterized by the presence of a simple electron in the 4f orbital. Ceria exhibits a large deviation from its CeO_2 stoichiometric composition by the creation of oxygen vacancies.[7−10] This property is the main reason that ceria is widely used as a support in catalysis.

When Cu^{2+} ions were added to CeO_2 and calcined under air at different temperatures, monomers, dimers, and clusters of Cu^{2+} were formed in the solid.[11−13] Cu^{2+}

* Corresponding author: E-mail: abiaad@univ-littoral.fr.

(1) Bond, G. C.; Perez Zurita, J.; Flamerz, S. *Appl. Catal.* **1986**, *27*, 353.
(2) Haller, G. L.; Resasco, D. E. *Adv. Catal.* **1987**, *108*, 364.
(3) Wainwright, M. S.; Trimm, D. L. *Catal. Today* **1995**, *23*, 29.
(4) Boccuzzi, F.; Chiorino, A.; Martra, G.; Gargano, M.; Ravasio, N.; Corrozzini, B. *J. Catal.* **1997**, *165*, 129 and references therein.
(5) Decarne, C.; Abi-Aad, E.; Aboukaïs, A. *Catal. Lett.* **1999**, *62*, 45.
(6) Abi-Aad, E.; Bechara, R.; Grimblot, J.; Aboukaïs A. *Chem. Mater.* **1993**, 5, 6, 793.
(7) Harrison, P. G.; Creaser, D. A.; Wolfindale, B. A.; Waugh, K. C.; Morris, M. A.; Mackrodt, W. C. In *Catalytic Surface Characterisation*; Dines, T. J., Rochester, C. H., Thomson, T., Eds.; Royal Society of Chemistry: Cambridge, 1992; 76.
(8) Otsuka, K.; Hatano, M.; Morikawa, A. *J. Catal.* **1983**, *79*, 493.
(9) Körner, R.; Ricken, N.; Nölting, J.; Riess, I. *J. Solid State Chem.* **1989**, *78*, 136.
(10) Brauer, G.; Gingerich, A.; Holtzchmidt, U. *J. Inorg. Nucl. Chem.* **1960**, *16*, 77.
(11) Soria, J.; Conesa, J. C.; Martinez-Arias, A.; Coronado, J. M. *Solid States Ionics* **1993**, *63−65*, 755.
(12) Aboukaïs, A.; Bennani, A.; Aïssi, C. F.; Wrobel, G.; Guelton, M.; Védrine, J. C. *J. Chem. Soc., Faraday Trans.* **1992**, *88*(4), 615.
(13) Aboukaïs, A.; Bennani, A.; Aïssi, C. F.; Wrobel, G.; Guelton, M. *J. Chem. Soc., Faraday Trans.* **1992**, *88* (9), 1321.

10.1021/cm000043e CCC: $20.00
Published on Web 09/20/2001

ion dimers were located in distorted octahedral sites. A highly mobile oxygen species was responsible for the coupling between the two Cu^{2+} ions. When the Cu/Ce atomic ratio is >0.5, two phases, CeO_2 and CuO, were formed. In such an oxidized state, the valences of copper and cerium are respectively +2 and +4.

If vanadium was impregnated on ceria, the formation of the $CeVO_4$ phase from CeO_2 and V_2O_5 occurred via an intermediate in which an unpaired electron was trapped in the V_2O_{5-x}/CeO_{2-y} system at high temperature.[14,15] The trapped electron was responsible for the reduction of Ce^{4+} to Ce^{3+}, whereas V^{5+} remained intact.

Ceria and transition oxides such as CuO and V_2O_5 are commonly used as catalysts in depollution reactions. Several investigations[16,17] showed that these three oxides were active in the catalytic combustion of carbon particulate coming from diesel exhaust. In our laboratory, a study of a CeO_2-supported copper system demonstrated that the presence of CuO induced a promoting effect on activity and CO_2 selectivity.[18] Furthermore, it is well-known that vanadium-based catalysts are very active for catalytic reduction of nitric oxides.[19,20]

Our work consisted of synthesizing different oxides constituted by cerium, copper, and vanadium in order to combine the physicochemical and catalytic properties of these three elements in the same solid. X-ray diffraction, thermal analysis, and electron paramagnetic resonance were used to characterize the Cu−V−Ce oxides and to evaluate the effect of the used precursors on the physicochemical properties of the solids.

Experimental Section

Ceria (CeO_2) was prepared by calcinating cerium hydroxide at 700 °C for 4 h under a flow of dried air. The latter solid was synthesized by precipitation from cerium(III) nitrate hexahydrate [$Ce(NO_3)_36H_2O$] with a concentrated NaOH solution at room temperature.

Subsequently, solutions of copper(II) nitrate [$Cu(NO_3)_2$-$3H_2O$] or/and vanadyl oxalate (VOC_2O_4) were impregnated on ceria. Different samples were synthesized with the following atomic ratios: Cu/Ce = 0.1 and V/Ce = 0.1. The freshly prepared solids were dried in a drying oven at 100 °C for 24 h and then calcined at 200 and 300 °C under a flow of air for 4 h. The oxides obtained were denoted as 1V10Ce, 1Cu10Ce, and 1Cu1V10Ce, where the number preceding the atom represents its atomic ratio in these samples.

X-ray powder diffraction analysis was carried out on a D5000 Siemens diffractometer equipped with a copper anticathode and a secondary beam monochromator. The X-ray diffraction (XRD) plots were recorded at room temperature.

Thermal analysis measurements were performed on a NETZSCH STA 409 apparatus. For each dried solid, a mass of 50 mg was considered and placed in a Al_2O_3 crucible. Simultaneous thermogravimetric−differential scanning calorimetric (TG−DSC) curves were obtained while samples were heated from 50 to 700 °C with a rate of 5 °C min^{-1} under a flow of air.

The electron paramagnetic resonance (EPR) measurements were performed at −196 °C on a EMX BRUKER spectrometer with a cavity operating at a frequency of ~9.5 GHz (X band). The magnetic field was modulated at 100 kHz. The *g* values were determined from precise frequency and magnetic field values. The calculated spectra were simulated with the BRUKER Simfonia program based upon perturbation theory.[21]

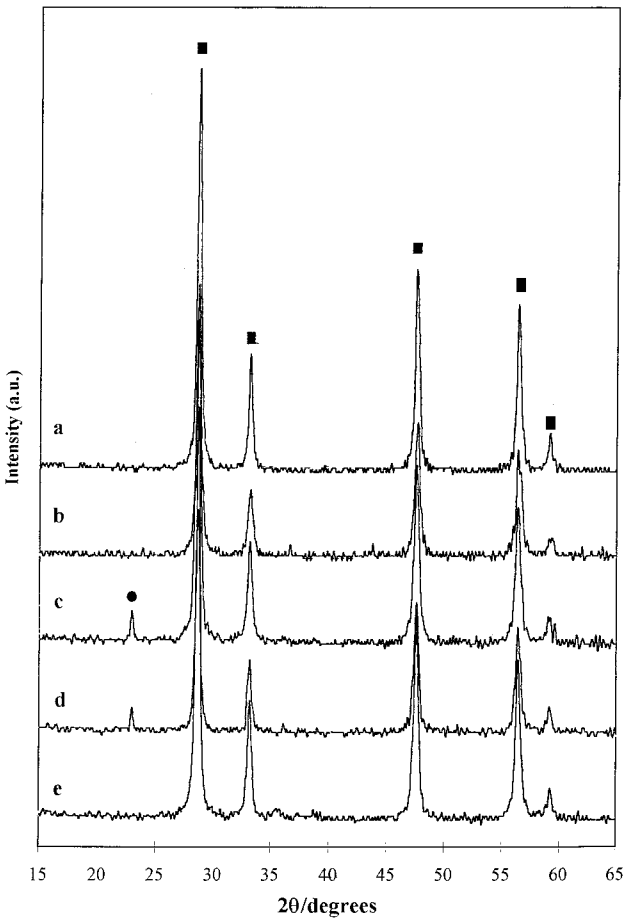

Figure 1. X-ray diffraction patterns of (a) dried 1V10Ce, (b) dried 1Cu10Ce, (c) dried 1Cu1V10Ce, (d) 1Cu1V10Ce calcined at 200 °C, and (e) 1Cu1V10Ce calcined at 300 °C (●, copper oxalate phase; ■, ceria phase).

Results and Discussion

X-ray Diffraction. Figure 1 shows the XRD patterns obtained for the different samples previously dried at 100 °C. A ceria phase (CeO_2) was found to be present in all the solids. However, for 1Cu1V10Ce sample, a diffraction line at $2\theta = 22.84°$ was observed. According to the literature,[22,23] it appears to correspond to the most intense diffraction line of the copper oxalate phase. The oxalate ions are known to function as bis-bidentate ligands, and their coordination to two copper ions affords a wide variety of polynuclear compounds.[24−27] There are four types of polymerization:

(14) Cousin, R.; Dourdin, M.; Abi-Aad, E.; Courcot, D.; Capelle, S.; Guelton, M.; Aboukaïs, A. *J. Chem. Soc., Faraday Trans.* **1997**, *93*, 21, 3863.
(15) Cousin, R.; Courcot, D.; Abi-Aad, E.; Capelle, S.; Amoureux, J. P.; Dourdin, M.; Guelton, M.; Aboukaïs, A. *Colloids Surf. A* **1999**, *158*, 43.
(16) Lahaye, J.; Boehm, S.; Chambrion, Ph.; Ehrburger, P. *Combustion Flame* **1996**, *104*, 199.
(17) Fredrik Ahlström, A.; Ingemar Odenbrand, C. U. *Appl. Catal.* **1990**, *60*, 157.
(18) Pruvost, C.; Lamonier, J. F.; Courcot, D.; Abi-Aad, E.; Aboukaïs, A. *Studies in Surface Science and Catalysis* **2000**, *130*, 2159.
(19) Went, G. T.; Leu, L. J.; Rosin, R. R.; Bell, A. T. *J. Catal.* **1992**, *134*, 492.
(20) Lietti, L.; Forzatti, P. *J. Catal.* **1994**, *147*, 241.
(21) Weber, R. T. *WINEPR SIMFONIA manual*, ver 1.2; Brucker Instruments, Inc.; Billerica, Ma, 1995; and references therein.
(22) Donia, A. M. *Polyhedron* **1997**, *16*, 17, 3013.
(23) Donia, A. M.; Dollimore, D. *Thermochim. Acta* **1996**, *290*, 139.
(24) Fitzgerald, W.; Foley, J.; McSweeney, D.; Ray, N.; Sheahan, D.; Tyaga, S.; Hathaway, B.; Brien, P. O. *J. Chem. Soc., Dalton Trans.* **1982**, 1117.

(i) Linear chain structures are formed,[28] in which the bridging oxalate ions coordinate in a monodentate fashion. The elongated coordination sites are occupied by the other oxygen atoms of oxalate.

(ii) Each copper has a square-planar coordination geometry having bis-bidentate oxalate with adjacent copper ions bridge by a single oxalate ion.

(iii and iv) Extended linear chain systems are intriguing, concerning their magnetic behavior and thermal solid-state reaction. However, X-ray crystallographic structures of these linear array compounds are still lacking.

The intensity of the copper oxalate phase, in the 1Cu1V10Ce sample, decreased with increasing calcination temperature and completely disappeared at 300 °C (Figure 1e). Thus, the appearance of this phase at $2\theta = 22.84°$ corresponded to vanadyl substitution by a cupric ion during the synthesis of the solids. This result was verified by the XRD analysis of the precipitate coming from the mixture of copper nitrate and vanadyl oxalate. The XRD diagram obtained was similar to the copper oxalate one described in the literature.[22,23] For better comprehension and precise analysis of this phase, a solid was synthesized from a ceria support and freshly prepared copper oxalate according to the experimental protocol from Donia et al.[22,23] and is designated as 1Cu10Ce*.

Thermal Analysis. The TG−DSC curves of 1V10Ce, 1Cu10Ce, 1Cu10Ce*, and 1Cu1V10Ce are illustrated in Figure 2. Characteristics of these thermal data, i.e., mass loss and temperature of thermal phenomenon, are presented in Table 1.

For 1V10Ce solid, a weight loss of 1.65% associated with a broad endothermic phenomenon was evidenced at low temperature (<160 °C) and could correspond to the removal of water. The second weight loss of 3.75% between 160 and 300 °C was associated with an intense exothermic peak that could indicate the oxidation of the organic function of the VOC_2O_4 precursor. The difference between the experimental (3.75%) and the calculated weight (3.41%) loss was due in this case to an excess of oxalate ions used for the preparation of vanadyl oxalate. Finally, a slight weight loss of 0.14% obtained between 450 and 700 °C was ascribed to the formation of $CeVO_4$ from vanadium(V) oxide and ceria, and this is in agreement with our previous work on V−Ce−O catalysts using EPR and ^{51}V MAS NMR measurements.[14,15]

Concerning the 1Cu10Ce sample, removal of water was also observed at low temperature (<160 °C). From 160 to 240 °C, a rapid weight loss phenomenon associated with a sharp endothermic peak at 220 °C was followed by a slower rate of weight loss between 240 and 310 °C. This observation revealed the copper nitrate decomposition as a two-step transformation. From the related experimental data given in Table 1 and Figure 2, it could be deduced that copper nitrate was partially decomposed to copper oxide before the beginning of the TG−DSC experiment. This fact was clearly demonstrated as the calculated weight loss (5.66%) corresponding to the decomposition of $Cu(NO_3)_2$ to CuO was much higher than the experimental weight loss (2.70%) obtained for 1Cu10Ce solid. Indeed, it was experimentally verified that the drying treatment at 100 °C of a pure $Cu(NO_3)_2 3H_2O$ resulted in its partial decomposition.

The thermal analysis of the 1Cu1V10Ce solid presented a regular and slow weight loss of 2.8% occurring until 260 °C and then a markedly rapid loss corresponding to an exothermic decomposition that was achieved between 260 and 305 °C. The comparison of such TG−DSC curves with those relative to 1V10Ce and 1Cu10Ce solids did not show the successive decomposition of both vanadyl oxalate and copper nitrate. The XRD data evidenced the presence of a CuC_2O_4 phase in the dried 1Cu1V10Ce solid. In fact, during the preparation of the solid, the presence in solution of Cu(II) ions with oxalate anions from VOC_2O_4 proceeded to the formation of copper oxalate CuC_2O_4. The latter compound is thermodynamically favored under these conditions, as the value of Gibbs energy under standard conditions of 298 K is -53.36 kJ mol^{-1}.[29,30]

The 1Cu10Ce* solid was studied by thermal analysis, and the TG curve showed a slight weight loss and then a plateau between 180 and 270 °C. The decomposition of oxalate functions from CuC_2O_4 occurred between 270 and 300 °C. The CuC_2O_4 clearly appeared much more stable than VOC_2O_4. Thus, the first continuous weight loss observed for the 1Cu1V10Ce sample up to 260 °C was attributed to the removal of water and the progressive decomposition of nitrate. It should be noted here that, in this case, the step characteristic of the nitrate decomposition with an endothermic peak at 220 °C, already evidenced in 1Cu10Ce, was not observed. The major pat of the nitrate ions were no longer associated with the copper(II) cations. Finally, the fast decomposition obtained between 260 and 305 °C corresponded to the oxidation of oxalate functions of CuC_2O_4 to yield copper oxide.

In conclusion, the XRD and the TG−DSC results showed that the solutions of copper nitrate and vanadyl oxalate, when simultaneously impregnated on ceria, formed a copper oxalate phase. To investigate the insertion of copper and vanadium ions in the CeO_2 matrix, an EPR study was performed.

EPR. Figure 3 shows the EPR experimental spectra obtained for all the dried samples: 1Cu1V10Ce, 1V10Ce, 1Cu10Ce, and 1Cu10Ce*.

The EPR parameter values of the different signals were determined from the calculated spectra. Simulated signals were calculated using the effective spin Hamiltonian

$$\mathcal{H} = \beta H_j S_j g_j + A_j S_j I_j$$

where j is the component along one of the three axis x, y, and z, H is the applied magnetic field, S is the total spin electron, A is the hyperfine interaction, I is the spin nuclear, g is the spectroscopic factor, and β is the Bohr

(25) Bloomquist, D. R.; Hansen, J. J.; Landee, C. P.; Willett, R. D.; Buder, R. *Inorg. Chem.* **1981**, *20*, 3308.
(26) Chananont, P.; Nixon, P. E.; Waters, J. M.; Waters, T. N. *Acta Crystallogr.* **1980**, *B36*, 2145.
(27) Gleizes, A.; Maury, F.; Galy, J. *Inorg. Chem.* **1980**, *19*, 2074.
(28) Garaj, J. *J. Chem. Soc. Chem. Commun.* **1968**, 904.
(29) Wagman, D. D.; Evans, W. H.; Parker, V. B.; Schumm, R. H.; Halow, I.; Churney, K. L.; Nuttall, R. L. *NBS Tables Chem. Thermodyn. Properties, J. Phys. Chem. Ref. Data*, **1982**, *11*, Suppl. 2.
(30) Garvin, D.; Parker, V. B.; White, H. J. *CODATA Thermodynamic Tables*; Hemisphere, New York, 1987.

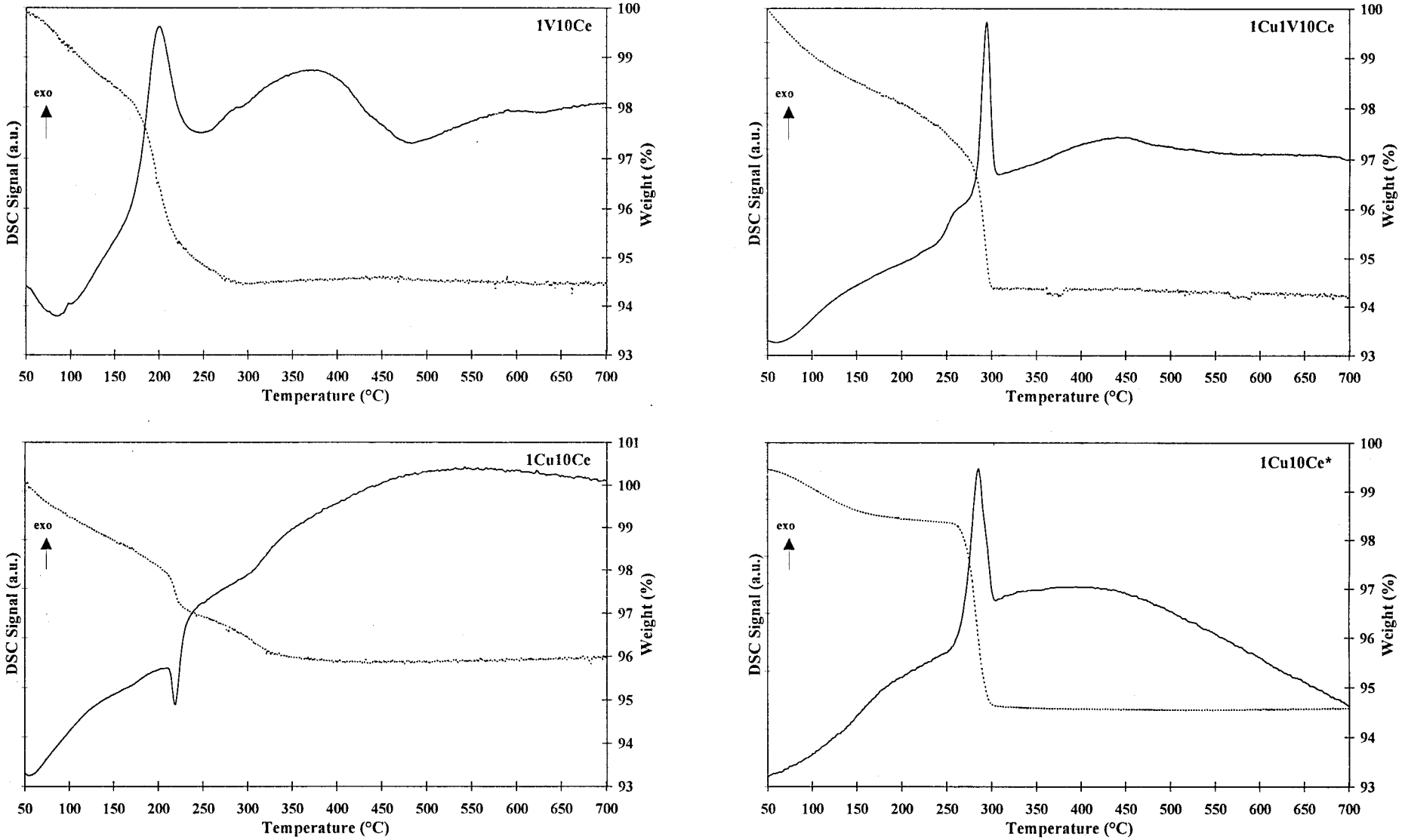

Figure 2. Thermal decomposition, under air: TG (---) and DSC (—) of the dried samples. Heating rate, 5 °C min^{-1}.

Table 1. Thermogravimetric Data of Solids and Their Attribution

	experimental data		attribution	
sample	temp (°C)	wt loss (%)	transformation	calcd wt loss (%)
1V10Ce	50−160	1.65	water removal	
	160−300	3.75	$VOC_2O_4 \rightarrow V_2O_5$	3.41
	450−700	0.14	$V_2O_5 + CeO_2 \rightarrow CeVO_4$	0.44
1Cu10Ce	50−160	1.80	water removal	
	160−350	2.70	$Cu(NO_3)_2 \rightarrow CuO$	5.66
1Cu10Ce*	50−180	1.07	water removal	
	270−300	3.80	$CuC_2O_4 \rightarrow CuO$	3.84
1Cu1V10Ce	50−260	2.80	water removal and progressive decomposition of nitrate	
	260−305	3.10	$CuC_2O_4 \rightarrow CuO$	3.49

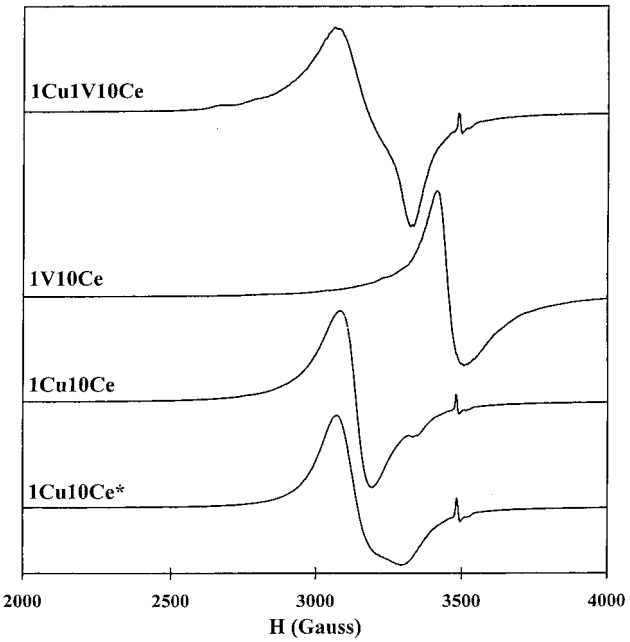

Figure 3. Experimental EPR spectra recorded at −196 °C for the dried samples.

magneton. A polyoriented sample EPR signal was simulated by generating 9000 random orientations of magnetic field and by summing the corresponding 9000 absorption signals. The final signal was obtained by performing a convolution (Gaussian or Lorentzian line shape) of each transition line, adding all contributions, and calculating the first derivative of the signal; the line width ΔH_j for convolution was optimized in order to obtain the best accordance with the observed experimental values.

The 1Cu1V10Ce experimental EPR spectrum (Figure 3) is the superimposition of several signals with different g values in the range of $g \approx 2$. To analyze this complex spectrum and to ascribe its signals, the EPR spectra of the binary compounds 1V10Ce, 1Cu10Ce, and 1Cu10Ce* were studied under the same conditions.

1V10Ce. The EPR spectrum of the 1V10Ce sample is the superimposition of three signals (Figure 4 and Table 2) corresponding to different V(IV) species. However, the spectral parameters of these signals were rather similar (Table 2). The observation of a broad axial signal without hyperfine structure, denoted by V_1 (Table 2), was due to strong dipolar interactions between the paramagnetic ions and revealed the presence of VO^{2+} agglomerates in the solid. Its high relative intensity (77.6%) indicated that these species were the most important participant. An isotropic broad signal denoted by V_2 (Table 2) was also observed and could be attributed to thick vanadyl agglomerate. Finally, an axial symmetry signal (V_3) with hyperfine structure, revealed by the eight parallel and perpendicular components (nuclear spin $I = {}^7/_2$), indicated the presence of a small amount (10.3% of the total intensity) of isolated V(IV) species dispersed on ceria. In this case, information about their environment can be obtained from g and A values (Table 2), indeed, $g_{iso} = 1.968$ and $A_{iso} = 117.6$ G. These values could correspond to VO^{2+} ions in octahedral symmetry axially distorted since $1.955 < g_{iso} < 1.980$ and $80 \text{ G} < A_{iso} < 120$ G.[31] Generally, lower g_{iso} and A_{iso} values are expected in the case of V^{4+} species in octahedral symmetry $1.920 < g_{iso} < 1.950$ and $60 \text{ G} < A_{iso} < 90$ G.[32−35]

1Cu10Ce. The simulation of the 1Cu10Ce EPR spectrum (Figure 4) revealed the presence of four signals. Table 3 shows their different parameters and the relative intensities. Two signals with g values >2 were characteristic of a d^9 electronic configuration (Cu^{2+} ions). An isotropic broad signal (Cu_1) centered at $g = 2.181$ with a line width of 117 G and a relative intensity of 78.7% (90.6% of the EPR detected copper) was due to copper nitrate agglomerations on ceria. Indeed, in such agglomerates the distance between the Cu^{2+} cations is very short, leading to high dipolar interactions and consequently to the broadness of the EPR signal. In addition, the thermal analysis data (Table 1) showed that the amount of water in this dried sample was about 1.8%. It is well-kwon that water molecules are very polar and their interaction with copper nitrate would increase the dipolar interactions and the broadness of the EPR signal. An axial symmetry signal (Cu_2) with hyperfine structure (nuclear spin $I = {}^3/_2$: $g_{||} = 2.312$, $g_{\perp} = 2.058$, $g_{iso} = 2.143$, $A_{||} = 130$ G, and $A_{\perp} = 21.7$ G) can be attributed to Cu^{2+} ions well-dispersed on ceria.[36] These copper species (Cu_2) might be related to the partial decomposition of the nitrate precursor at 100 °C observed by thermal analysis. The Cu_2 EPR parameters indicate that the corresponding Cu^{2+} ions are in a tetragonally distorted octahedral crystal field and they are surrounded by less than six ligands.[37] Under these

(31) Takahashi, H.; Shiotani, M.; Kobayashi, H.; Sohma, J. *J. Catal.* **1969**, *14*, 134.
(32) Centi, G.; Perathoner, S.; Trifiro, F.; Aboukaïs, A.; Aïssi, C. F.; Guelton, M. *J. Phys. Chem.* **1992**, *96*, 2617.
(33) Davidson, A.; Che, M. *J. Phys. Chem.* **1992**, *96*, 9909.
(34) Bogomolova, L. D.; Khabarova, A. N.; Klimashina, E. V.; Krasil'nikova, N. A.; Jachkin, V. A. *J. Non-Cryst. Solids* **1988**, *103*, 319.
(35) Cavani, F.; Centi, G.; Foresti, E.; Trifiro, F.; Busca, G. *J. Chem. Soc., Faraday Trans.* **1988**, *84*, 237.
(36) Aboukaïs, A.; Bennani, A.; Lamonier − Dulongpont, C.; Abi-Aad, E.; Wrobel, G. *Colloids and Surfaces A* **1996**, *115*, 171.

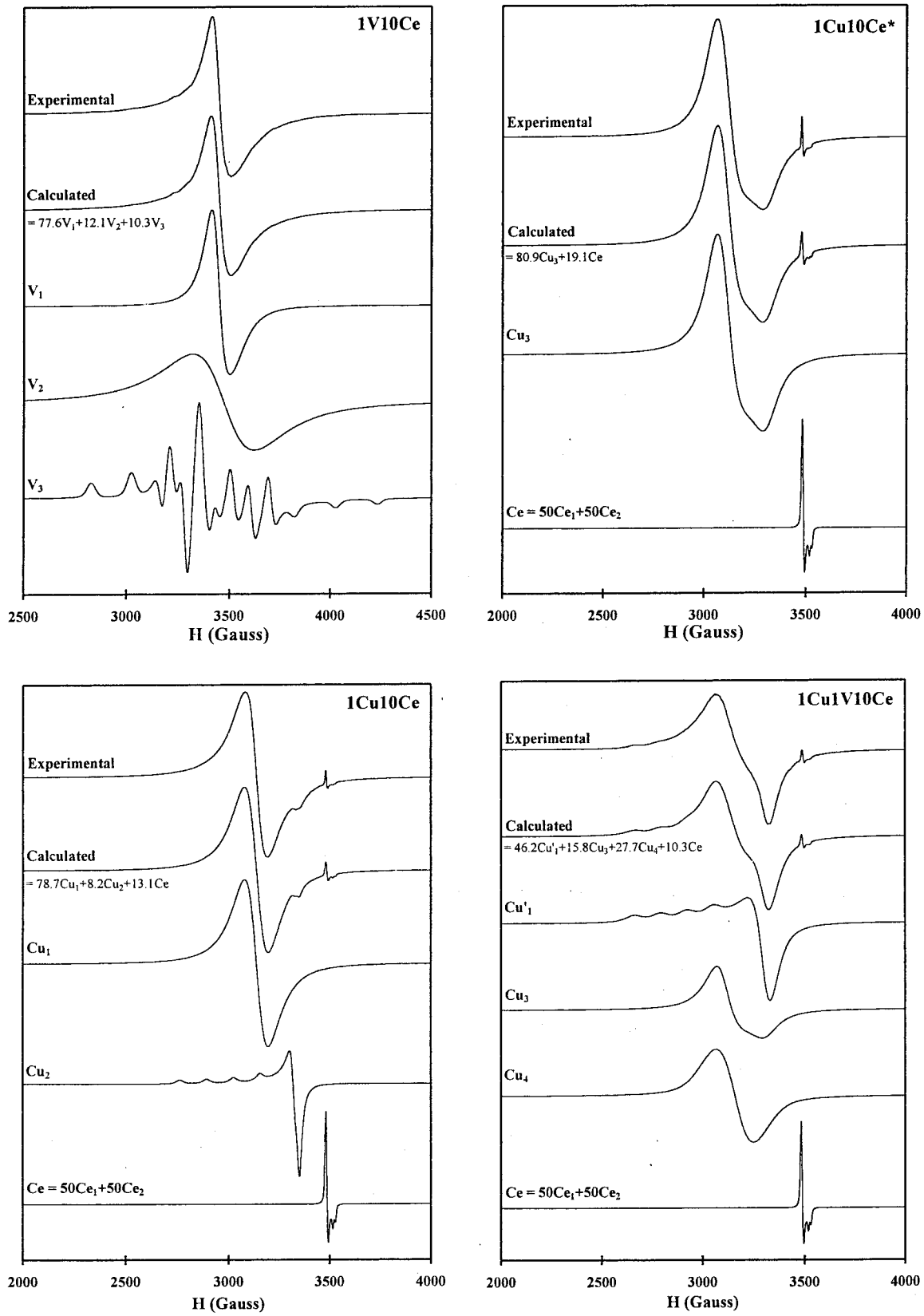

Figure 4. Calculated EPR signals from cerium, copper, and vanadium species and their summation with respect to relative intensities to give simulated spectra.

conditions, the isolated Cu^{2+} species (Cu_2) are bonded to the lattice oxygen of the support. Consequently, their coordination sphere, containing some support oxygen, is different from those of copper nitrate agglomerations, which could explain the difference in the EPR parameters of Cu_1 and Cu_2 signals. The intensity of the Cu_2 signal represented about 9.4% of the total detected

(37) Martini, G.; Basseti, V.; Ottaviani, M. F. *J. Chim. Phys.* **1980**, *77*, 311.

Table 2. EPR Parameters of the Different Signals Observed for the Dried 1V10Ce Sample[a]

signal	$g_{\|\|}$	$g_{\perp}$	g_{iso}	$A_{\|\|}$	$A_{\perp}$	$\Delta H_{\|\|}$	$\Delta H_{\perp}$	%
V_1	1.937	1.989	1.972			115	64	77.60
V_2			1.970			300	300	12.10
V_3	1.935	1.985	1.968	201	76	40	35	10.30

[a] A and ΔH values are given in G.

Table 3. EPR Parameters of the Different Signals Observed for the Dried 1Cu10Ce Sample[a]

signal	$g_{\|\|}$	$g_{\perp}$	g_{iso}	$A_{\|\|}$	$A_{\perp}$	$\Delta H_{\|\|}$	$\Delta H_{\perp}$	%[b]
Cu_1			2.181			117	117	78.7 *(90.6)*
Cu_2	2.312	2.058	2.143	130	21.7	25	20	8.2 *(9.4)*
Ce_1	1.947	1.965				8	10	6.55
Ce_2	1.941	1.965				8	10	6.55

[a] A and ΔH values are given in G. [b] The percent of total detected copper is in italic type.

copper. Thus, it is important to remember that the intensity of the EPR signal from isolated Cu^{2+} ions may be regarded as a measure of the degree of oxidation of the catalyst. Nevertheless, the formation of CuO crystallites on the catalyst surface can decrease the effective intensity of the isolated Cu^{2+} signal. Berger et al.[38] have shown that the observed EPR intensity is a percentage of the theoretical total intensity due to nearly isolated Cu^{2+} ions only. Kucherov et al.[39] have used frozen water solutions of $CuSO_4$ in order to estimate the cupric ions concentration. Reliable results have been obtained for 1.27 wt % Cu introduced into ZSM-5 by ion exchange, where the EPR signal was representative of almost all the Cu^{2+} ions in the sample. Nevertheless, when the Cu content increases (∼5 wt %), the EPR-detectable Cu^{2+} fell to about 55%.[40] Thus, the intensity is also correlated with the concentration and dispersion of the copper(II) species. The lower the degree of dispersion, the larger the fraction of copper that escapes detection by EPR. In the thermal analysis study exposed in this work, it has been demonstrated that copper nitrate was partially decomposed into copper oxide during the drying stage at 100 °C. From the data reported in Table 1, this part can be estimated to 52.3% of the total copper nitrate, whereas the EPR results specify that 90.6% of the copper(II) species are in copper nitrate agglomerates and only 9.4% as Cu^{2+} ions well-dispersed on ceria. Thus, the possibility that part of the copper cations might be EPR silent should not be omitted. In fact, the copper content in the 1Cu10Ce sample is equal to 3.33 wt % Cu, and according to experimental protocol from Kucherov et al.,[39] the estimate of detected EPR copper represents more than 88%. The EPR intensities, used for this purpose, were calculated from the double integration of the corresponding EPR signals and normalized with respect to the recording conditions.

Two other signals with g values <2 were observed and designated as Ce_1 and Ce_2 (Table 3). Similar signals were observed in the literature[6,43] and assigned to an interaction between conduction electrons and the vacant orbitals of Ce^{4+} ions in the CeO_2 matrix. It is important to notice that these signals were also present on the EPR spectrum of the ceria support before the impregnation of vanadium or/and copper salts.

*1Cu10Ce**. The EPR spectrum of the 1Cu10Ce* sample is the superimposition of three signals (Figure 4). The same Ce_1 and Ce_2 signals, corresponding to the ceria support, were observed in this case with a relative intensity of 19.1%. Consequently, 80.9% of the total intensity (100% of the copper compounds) was due to an axial symmetry signal Cu_3: $g_{\perp} = 2.209$ and $g_{\|} = 2.071$ (Figure 4). This latter signal can be, without ambiguity, attributed to Cu^{2+} ions, as copper oxalate compounds, despite the fact that $g_{\perp} > g_{\|}$. The inversion in g anisotropy values has already been observed in the copper EPR studies.[44−47] According to the Jahn−Teller theorem, copper(II) complexes can never be rigorously octahedral. The idealized geometry must be tetragonally distorted, and this distortion can result either in the elongation or in the compression of the octahedron. In principle, EPR spectroscopy can distinguish between these: $g_{\|} > g_{\perp}$ for elongation and $g_{\|} < g_{\perp}$ for compression. However, these patterns are only trends if the complexes are magnetically dilute, since exchange interactions tend to average EPR spectra, and therefore, crystal g tensors are not necessarily the same as molecular g tensors. Certain authors[48−50] have taken $g_{\|} > g_{\perp}$ to be typical when the ground state of the unpaired spin is $d_{x^2-y^2}$. This situation appears when the coordination geometry is a tetragonally elongated octahedral, square pyramidal, or square planar. The inverted signals ($g_{\perp} > g_{\|}$) are generally obtained when the ground state is d_{z^2} and appear when the coordination geometry is a tetragonally compressed or rhombohedrally distorted octahedron, tetragonally elongated tetrahedron, cis-distorted octahedron, or trigonal bipyramidal configuration. Copper oxalate is manifested by the different structures mentioned above. It appears that the first, which is constituted by a linear chain of oxalate ions and coordinated in a monodentate fashion, is the more probable form of the copper oxalate but with rather compressed coordination sites than elongated versions.[24−28] Furthermore, the unpaired electron is localized in the d_{z^2} orbital and not in the $d_{x^2-y^2}$ orbital of Cu^{2+} ions. This compressed coordination can be due to the Cu^{2+} ion's radius value (0.73 Å), which is relatively higher than that of the V^{4+} ion (0.58 Å). Indeed, the EPR signal of the latter species (Figure 4) has normal values of $g_{\|}$ and $g_{\perp}$ in the oxalate phase with an elongated octahedral symmetry. Consequently, the substitution of V^{4+} by Cu^{2+} ions, with a larger ionic radius, leads to an octahedral symmetry of Cu^{2+} ions with a compression

(38) Berger, P. A.; Roth, J. F. *J. Phys. Chem.* **1967**, *71*, 4307.
(39) Kucherov, A. V.; Gerlock, J. L.; Jen, H.-W.; Shelef, M. *J. Phys. Chem.* **1994**, *98*, 4892.
(40) Lo Jacono, M.; Fierro, G.; Dragone, R.; Feng, X.; d_Itri, J.; Hall, W. K. *J. Phys. Chem.* **1997**, *101*, 1979.
(41) Kucherov, A. V.; Gerlock, J. L.; Jen, H.-W.; Shelef, M. *J. Catal.* **1995**, *152*, 63.
(42) Soria, J.; Martinez-Arias, A.; Martinez-Chaparro, A.; Conesa, J. C.; Schay, Z. *J. Catal.* **2000**, *190*, 352.
(43) Oliva, C.; Termignonne, G.; Vatti, F. P.; Forni, L.; Vishniakov, A. V. *J. Materials Science* **1996**, *31*, 6333.
(44) Herman, R. G. *Inorg. Chem.* **1979**, *18*, 995.
(45) Hughey, J. L.; Fawcett, T. G.; Rudich, S. M.; Lalancette, R. A.; Potnza, J. A.; Schugar, H. J. *J. Am. Chem. Soc.* **1979**, *101*, 2617.
(46) Bencini, A.; Gatteschi, D. *J. Magn. Reson.* **1979**, *34*, 653.
(47) Bencini, A.; Bertini, I.; Gatteschi, D.; Scozzafava, A. *Inorg. Chem.* **1978**, *17*, 3194.
(48) Hathaway, B. J., Billing, D. E. *Coord. Chem. News* **1970**, *5*, 143.
(49) Hoffman, S. K.; Goslar, J. *J. Solid State Chem.* **1982**, *44*, 343.
(50) Corma, A.; Pérez-Pariente, J.; Soria, J. *Clay Miner.* **1985**, *20*, 46.

Table 4. EPR Parameters of the Different Signals Observed for the Dried 1Cu1V10Ce Sample[a]

signal	$g_{\|\|}$	$g_{\perp}$	g_{iso}	$A_{\|\|}$	$A_{\perp}$	$\Delta H_{\|\|}$	$\Delta H_{\perp}$	%[b]
$Cu_{1'}$	2.398	2.075	2.182	130	24.3	65	73	46.2 *(51.5)*
Cu_3	2.071	2.209	2.163			95	103	15.8 *(17.6)*
Cu_4			2.168			170	170	27.7 *(30.9)*
Ce_1	1.947	1.965				8	10	5.15
Ce_2	1.941	1.965				8	10	5.15

[a] A and ΔH values are given in G. [b] The percent of total detected copper is in italic type.

of oxygen atoms and the inverted g values of the Cu^{2+} EPR signal.

Finally, it is important to note that no Cu^{2+} signals with resolved hyperfine structure, relative to isolated Cu^{2+} ions, were detected for the 1Cu10Ce* EPR spectrum. In addition, from the Cu^{2+} EPR signal intensity, the detected part is estimated to be 56%, considerably lower than in the case of the 1Cu10Ce sample, whereas the copper content is almost the same (3.39 wt % Cu).

1Cu1V10Ce. The simulated signals of the 1Cu1V10Ce EPR spectrum are shown in Figure 4, and their parameters are listed in Table 4. The addition of five signals with different relative intensities were necessary to have a faithful reproduction of the experimental spectrum. Three of these signals were characteristic of the Cu(II) species in a different environment and the two others were attributed to the cerium species previously described.

The first signal, denoted by Cu_1' (Figure 4), presented an axial symmetry with $g_{\|} = 2.398$, $g_{\perp} = 2.075$, $g_{iso} = 2.182$, $A_{\|} = 130$ G, and $A_{\perp} = 24.3$ G. Similar spin-Hamiltonian parameters have been reported[12,36−42] for distorted octahedral complexes in different matrices where the surrounding ligands might be inequivalent atoms or molecules. Nevertheless, distorted octahedral symmetry may be expected even for completely hydrated Cu^{2+} ions where all of the Cu^{2+} are EPR active.[40] Comparing with the literature data and the EPR spectrum of the 1Cu10Ce sample, this signal can be attributed to well-dispersed copper nitrate species on ceria. However, in this case, the relative intensity of the signal (46.2%) was considerably smaller than that observed for the 1Cu10Ce sample (78.7%). Moreover, the thermogravimetric data (Table 1) showed that the weight losses corresponding to the removal of water and the nitrate decomposition were 4.5% and 2.8% for 1Cu10Ce and 1Cu1V10Ce, respectively. Thus, the water and the nitrate contents are considerably higher on the 1Cu10Ce sample, which would increase the dipolar interactions and the broadness of the EPR lines. In addition, it has been demonstrated, in the thermal analysis part of this work, that the interaction between the nitrate ions and the Cu^{2+} cations was attenuated in the case of the ternary sample. Consequently, these experimental facts resulted in the decrease of the components line width of the Cu_1' signal comparing to the Cu_1 signal (Tables 3 and 4) and permitted the observation of the hyperfine structure; nevertheless, the g_{iso} value was the same in both cases.

In addition to the inverted axial signal Cu_3 (Figure 4) characteristic of the copper oxalate Cu^{2+} ions, an isotropic signal denoted by Cu_4 (Figure 4; Table 4) and centered at $g = 2.168$ was observed. Owing to its EPR parameters, this signal can be attributed to agglomerates of copper oxalate on ceria. Thus, Cu_3 and Cu_4 signals were both assigned to copper oxalate species in agglomerate form. Nevertheless, the Cu_4 signal was originated by interacting copper oxalate clusters of larger size than those responsible for the Cu_3 signal, which induce high dipolar interaction and the broadness of the EPR lines. In addition, it could be assumed that the Cu^{2+} species responsible for the Cu_4 signal are located in spherical-like symmetry, since the resulting EPR signal is isotropic. This Cu_4 signal was not observed in the EPR spectrum of the 1Cu10Ce* sample. Thus, the agglomeration of the copper oxalate species could result from the presence of vanadium compounds, influencing the environment of the copper oxalate, or from the simultaneous presence of copper nitrate species that were highly dispersed in this case (Cu_1' signal).

The relative intensity of these Cu_3 and Cu_4 signals, corresponding to copper oxalate species, presented 48.5% of the total EPR detected copper(II). This value is very similar to that obtained for the Cu_1' signal (51.5%) relative to the copper nitrate compounds. Thus, in this case (1Cu1V10Ce sample), one can deduce that about half the impregnated copper nitrate on ceria was transformed to copper oxalate. These latter anions (oxalate) were provided by the vanadyl oxalate salt. These results are in perfect agreement with those of thermal analysis and XRD exposed in this work. However, it should be mentioned here that part of the copper cations could be EPR silent. In fact, the copper content is 3.08 wt % Cu in the 1Cu1V10Ce sample, and according to the experimental protocol of Kucherov et al.,[39] the detected copper part from EPR intensity represents about 71%.

Finally, it is important to note that no signals relative to V(IV) species were detected in the 1Cu1V10Ce EPR spectrum. In this case, the V^{5+} ions appeared to be stabilized by the presence of the copper compounds, since in the 1V10Ce EPR spectrum three signals characteristic of different V(IV) species were detected.

General Discussion. The two EPR signals showing hyperfine structures, Cu_2 and Cu_1, are both assigned to well-dispersed Cu^{2+} cations on ceria support and related to the use of copper nitrate salt. Indeed, no Cu^{2+} EPR signals relative to isolated Cu^{2+} ions were detected for the 1Cu10Ce* sample, synthesized from ceria support and freshly prepared copper oxalate. Thus, it can be deduced that the dispersion of the copper(II) cations over the ceria support surface is facilitated with the copper nitrate precursor. This feature could be related to the coordination geometry, which is tetragonally elongated ($g_{\|} > g_{\perp}$) when the Cu^{2+} ions are present as copper nitrate phase, CuO phase, or well-dispersed in the CeO_2 matrix,[36] whereas, this geometry is tetragonally compressed ($g_{\perp} > g_{\|}$) in the case of copper oxalate. Moreover, the part of the copper cations detected by EPR from 1Cu10Ce, 1Cu1V10Ce, and 1Cu10Ce* samples represents 88%, 71%, and 56%, whereas the copper contents are 3.33%, 3.08%, and 3.39%, respectively. These results clearly show that the increase of the oxalate precursor content induces a large fraction of copper that escapes detection by EPR. This undetectable part could be consistent with the presence of large Cu(II) agglomerates.[38] In addition, the thermal analysis data clearly showed that the copper oxalate compounds

Table 5. EPR Parameters of Cu(II) Species for 1Cu10Ce, 1Cu10Ce*, and 1Cu1V10Ce Solids Calcined at 300 °C[a]

signal	$g_{\|\|}$	$g_{\perp}$	g_{iso}	$A_{\|\|}$	$A_{\perp}$	DI/N
1Cu10Ce	2.321	2.032	2.128	131	27.5	224
1Cu10Ce*	2.316	2.034	2.128	129	27.5	100
1Cu1V10Ce	2.364	2.046	2.152	131	26.2	140

[a] *A* values are given in G. EPR intensity is calculated from normalized double integration (arbitrary unit).

are decomposed at higher temperature than the copper nitrate ones. This higher stability of the copper oxalate species could inhibit their interaction with the ceria support surface in the low-temperature range (<300 °C).

After the calcination at 300 °C of the dried solids, all the recorded EPR spectra are the superimposition of three signals: Ce_1 and Ce_2 relative to the ceria support and a third one characteristic of Cu(II) species. The EPR parameters of this latter signal are reported in Table 5 for the three copper-containing samples. It is clear that the EPR parameters of the Cu(II) species were very similar for the two binary compounds 1Cu10Ce and 1Cu10Ce*, whereas for the 1Cu1V10Ce sample, the parameters were significantly different. Moreover, the EPR parameters observed for the two binary samples were very similar to those of Cu_2 signal assigned to well-dispersed Cu^{2+} ions on ceria and issued from the partial decomposition of the nitrate precursor at the drying stage. These results confirmed the assignment of the Cu_2 signal. In all cases, the Cu(II) species were located in octahedral sites tetragonally distorted and surrounded by less than six ligands.[37] However, for the 1Cu1V10Ce sample, the distortion seemed to be more pronounced than in the case of the two binary samples. This phenomenon may result from the presence of the vanadium (V) species present in the solid and detected by ^{51}V MAS NMR[15].

Finally, after the decomposition of the copper nitrate or oxalate salts, it appears that the precursors have no influence on the environment symmetry of the EPR-detected copper species. Nevertheless, an important feature should be noted with regard to the EPR intensities (Table 5). In agreement with the results discussed above, the EPR intensities clearly show that the EPR-detected part of the copper is significantly greater when the copper precursor is nitrate. Thus, it is clearly shown that the dispersion of the copper(II) cations over the ceria support surface is favored with the copper nitrate precursor, and consequently, the EPR intensity is considerably higher.

Conclusion

In this work, the influence of vanadyl and copper precursors on the physicochemical properties of binary and ternary V−Cu−Ce oxides was evaluated. The formation of a copper oxalate phase from copper nitrate and vanadyl oxalate was revealed during the preparation of the 1Cu1V10Ce ternary oxide. The EPR spectra relative to the dried copper containing samples were the superimposition of several signals attributed to copper nitrate, copper oxalate, Cu^{2+} ions well-dispersed on ceria surface, and conduction electrons in interaction with the vacant orbitals of the Ce^{4+} ions. The copper oxalate phase exhibited a Cu(II) EPR signal with inverted *g*-values, related to the presence of compressed sites with an octahedral symmetry. Moreover, from the EPR data, it can be deduced that the dispersion of the copper-(II) cations over the ceria support surface was favored by the use of the copper nitrate as precursor. The EPR intensities clearly show that the increase of the oxalate precursor content induces a large fraction of copper that escapes detection by EPR and could be consistent with the presence of large Cu(II) agglomerates. After the calcination at 300 °C of the dried solids, the Cu(II) species were located in octahedral sites tetragonally distorted and surrounded by less than six ligands. However, for the 1Cu1V10Ce sample, the distortion appeared to be more important than that observed in the case of the two binary samples. Despite the fact that the EPR parameters of the Cu^{2+} ions were very similar, it was clearly shown that the high dispersion of the copper(II) cations over the ceria support surface, owing to the copper nitrate, was confirmed after the decomposition of the precursors.

Acknowledgment. The authors would like to thank the "Conseil Général du Nord", the "Région Nord−Pas de Calais", and the European Community (European Regional Development Fund) for financial support in the purchase of the EPR and thermal analysis apparatus.

CM000043E